



HAL
open science

Atmospheric Photosensitization: A New Pathway for Sulfate Formation

Xinke Wang, Rachel Gemayel, Nathalie Hayeck, Sébastien Perrier, Nicolas Charbonnel, Caihong Xu, Hui Chen, Chao Zhu, Liwu Zhang, Lin Wang, et al.

► **To cite this version:**

Xinke Wang, Rachel Gemayel, Nathalie Hayeck, Sébastien Perrier, Nicolas Charbonnel, et al.. Atmospheric Photosensitization: A New Pathway for Sulfate Formation. *Environmental Science and Technology*, 2020, 54 (6), pp.3114-3120. 10.1021/acs.est.9b06347 . hal-02566392

HAL Id: hal-02566392

<https://hal.science/hal-02566392v1>

Submitted on 18 Nov 2020

HAL is a multi-disciplinary open access archive for the deposit and dissemination of scientific research documents, whether they are published or not. The documents may come from teaching and research institutions in France or abroad, or from public or private research centers.

L'archive ouverte pluridisciplinaire **HAL**, est destinée au dépôt et à la diffusion de documents scientifiques de niveau recherche, publiés ou non, émanant des établissements d'enseignement et de recherche français ou étrangers, des laboratoires publics ou privés.

Atmospheric photosensitization: a new pathway for sulfate formation

Xinke Wang[†], Rachel Gemayel[†], Nathalie Hayeck[†], Sebastien Perrier[†], Nicolas Charbonnel[†],
Caihong Xu[‡], Hui Chen[‡], Chao Zhu[‡], Liwu Zhang[‡], Lin Wang[‡], Sergey A. Nizkorodov[§],
Xinming Wang^{||}, Zhe Wang[⊥], Tao Wang[⊥], Abdelwahid Mellouki[#], Matthieu Riva[†], Jianmin
Chen^{‡,¶,*}, Christian George^{†,*}

[†]Univ Lyon, Université Claude Bernard Lyon 1, CNRS, IRCELYON, F-69626, Villeurbanne, France.

[‡]Shanghai Key Laboratory of Atmospheric Particle Pollution and Prevention (LAP3), Department of Environmental Science & Engineering, Institute of Atmospheric Sciences, Fudan University, Shanghai 200438, China.

[§]Department of Chemistry, University of California, Irvine, Irvine, California, 92697, USA.

^{||}State Key Laboratory of Organic Geochemistry and Guangdong province Key Laboratory of Environmental Protection and Resources Utilization, Guangzhou Institute of Geochemistry, Chinese Academy of Sciences, Guangzhou 510640, China

[⊥]Department of Civil and Environmental Engineering, The Hong Kong Polytechnic University, Hong Kong, China.

[#]Institut de Combustion, Aérothermique, Réactivité et Environnement (ICARE), CNRS/OSUC, 45071 Orléans Cedex 2, France

[¶]Institute of Eco-Chongming, 3663 Zhongshan Road, Shanghai 200062, China

*To whom correspondence should be addressed. Email: christian.george@ircelyon.univ-lyon1.fr,

Email : jmchen@fudan.edu.cn

Abstract

Northern China is regularly subjected to intense wintertime “haze events”, with high levels of fine particles that threaten millions of inhabitants. While sulfate is a known major component of these fine haze particles, its formation remains unclear especially under highly polluted conditions, with state-of-the-art air quality models unable to reproduce or predict field observations. These haze conditions are generally characterized by simultaneous high emissions of SO₂ and photosensitizing materials. In this study, we find that the excited triplet states of photosensitizers could induce a direct photosensitized oxidation of hydrated SO₂ and bisulfite into sulfate S(VI) through energy transfer, electron transfer or hydrogen atom abstraction. This photosensitized pathway appears to be a new and ubiquitous chemical route for atmospheric sulfate production. Comparing to other aqueous-phase sulfate formation pathways with ozone, hydrogen peroxide, nitrogen dioxide, or transition metal ions, the results also show that this photosensitized oxidation of S(IV) could make an important contribution to aerosol sulfate formation in Asian countries, particularly in China.

Introduction

Fine particulate matter, a complex cocktail of inorganic and organic species, has a central role during persistent haze events in the North China Plain. While sulfate (SO₄²⁻) is ubiquitous and a key component, its production from SO₂ is still uncertain. While gaseous SO₂ can be oxidized through its reaction with OH radicals, it also undergoes significant multiphase processing through reactions involving a variety of dissolved oxidants such as ozone (O₃), hydrogen peroxide (H₂O₂), and transition metal ions (TMIs)¹⁻³. However, the detailed chemical mechanism under heavily polluted conditions remains uncertain. Current atmospheric observations highlighting high sulfate production during severe haze events⁴ cannot be reproduced by atmospheric models⁵. To close this

45 gap, new chemical pathways have been suggested involving an interfacial SO₂ oxidation on acidic
46 microdroplets⁶, SO₂ triplet state chemistry⁷⁻⁹ or oxidation at higher pH via a reaction with NO₂¹⁰,
47 ¹¹. In sum, despite intense research efforts, important missing processes hamper our abilities to
48 clearly elucidate the formation of one of the most important components of haze particles.

49 Photosensitized chemistry has been recently discussed as triggering novel chemistry in
50 tropospheric particles¹², but its role for S(IV) oxidation under polluted conditions has not been
51 explored. A photosensitizing molecule will absorb solar radiation and create an excited (triplet)
52 state T* from which various chemical pathways can be initiated that would otherwise not take
53 place at ground state¹³. Biomass burning for residential heating, typical for China during haze
54 events, are in fact a likely source of compounds bearing functional groups capable of
55 photosensitized oxidation as observed in HULIS (Humic Like Substances)¹⁴. We therefore
56 investigated whether photosensitized oxidation of SO₂ may occur under atmospheric conditions,
57 as an attempt to close some gaps in our knowledge of sulfate formation under polluted conditions.

58

59 **Materials and Methods**

60 All experiments were conducted at room temperature in the range of 295-300 K.

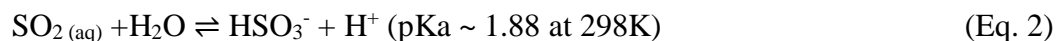
61 **Chemicals.** All chemicals were used as purchased: acetophenone (Sigma Aldrich, 98%),
62 flavone (Sigma Aldrich, ≥ 99.0%), xanthone (Sigma Aldrich, 97%), 4- (benzoyl)benzoic acid (4-
63 BBA, Sigma Aldrich, 99%), sodium sulfite (Sigma Aldrich, ≥ 98%), sulfuric acid (Sigma Aldrich,
64 95-97%), humic acid (HA, Sigma Aldrich, technical grade), humic acid salt (HAS, Sigma Aldrich,
65 technical grade). In addition, all solutions were freshly prepared using ultrapure water (Elga
66 Purelab Classic, 18.2 MΩ cm). In order to promote dissolution, 4-BBA solutions were stirred in
67 an ultrasonic bath for 10 min, and the solutions of xanthone and flavone were agitated for 2 hour

68 in the dark, both at ambient temperature. For the chromatographic analysis, acetonitrile, water and
69 formic acid were all three of Optima® LC/MS grade, provided by Fisher Scientific. O- (2,3,4,5,6-
70 pentafluorophenyl) methylhydroxyl amine hydrochloride (PFBHA, $\geq 99.0\%$) was also purchased
71 from Fluka. In addition, SO₂ (10 ppm, mixing with pure N₂, Linde, France) and N₂ (99.999%)
72 were used in this study.

73 **PM_{2.5} samples collection and extraction.** 24-hour ambient aerosol samples (PM_{2.5} masses in
74 the range of 27-46 mg) were collected onto 90 mm prebaked quartz-fiber filters (Whatman
75 Company, UK) during 10 to 14 December 2018, using a mid-volume sampler (TH-150A, Wuhan
76 Tianhong, China) operating at 100 L min⁻¹. The sampling site was located in rural Wangdu (38°42'
77 N, 115°08' E), Baoding, Hebei Province, surrounded by grasslands and farms, but easily
78 influenced by industrial and urban plumes from megacities such as Beijing, Tianjin, and
79 Shijiazhuang. After sampling, filters were stored at -20 °C in a freezer before further analysis.

80 Each quartz filter was extracted with three subsequent 15 mL extractions of ultrapure water and
81 agitated for 25 min on an orbital shaker set at 1000 rpm. After filtering through a 0.2 μm
82 polytetrafluoroethylene membrane (13 mm, Pall Corporation, USA) using a glass syringe, the
83 combined ambient aerosol extracts (AA as abbreviation) were used to conduct the photochemical
84 experiments described below. In addition, in order to characterize chromophores and carbonyl-
85 containing compounds, these extracts were analyzed by using a UPLC/DAD/(+/-)HESI-HRMS
86 platform, which is the combination of ultra-high performance liquid chromatography (UPLC,
87 Dionex 3000, Thermo Scientific, USA), a diode array detector (DAD), and an Orbitrap high
88 resolution mass spectrometer (HRMS, Q Exactive, Thermo Scientific, Bremen, Germany) using
89 heated electrospray ionization (HESI). More Information about chemical analysis of filter samples
90 were illustrated in the Supporting Information.

91 **Quartz cell experiments.** A 14 mL cylindrical quartz cell (5 cm length and 2 cm diameter)
92 mounted 13 cm away along its axis of a Xenon lamp (150 W; LOT-QuantumDesign, France) used
93 to perform the experiments. A quartz water filter of 5 cm length and a Pyrex filter were mounted
94 in front of the lamp to remove infra-red irradiation and short wavelengths ($\lambda < 290\text{nm}$). The
95 spectral characteristics of this system can be found in Figs. 5 of Ciuraru et al.¹⁵. In order to
96 maximize the surface to volume ratio ($1.4 \text{ cm}^2 \text{ cm}^{-3}$), the cell was half-filled with 7 mL of pure
97 water, $75 \mu\text{M}$ 4-BBA, 70 mg L^{-1} HA, 70 mg L^{-1} HAS, or AA (diluted by adding 1 mL ultrapure
98 water or water acidified with sulfuric acid (H_2SO_4) to a desired pH, see below), respectively. An
99 incoming diluted SO_2 gas flow (around 83 ppb after diluting by pure air) with a flowrate of 300
100 mL min^{-1} was injected through the cell and further diluted by adding 200 mL min^{-1} N_2 , then
101 analyzed afterwards by a SO_2 analyzer (Thermo, 43i). At the beginning of all experiments, higher
102 concentrations of SO_2 were injected into the reactor in order to more rapidly reach the SO_2
103 gas/liquid equilibrium. In other words, these solutions were pre-conditioned with flowing gaseous
104 SO_2 to establish Henry's law and acid-base equilibria producing hydrated SO_2 , HSO_3^- and SO_3^{2-} ,
105 according to Eqs. 1-3:



109 Sulfate concentrations in the liquid phase were measured using ion chromatography (IC,
110 Metrohm, 881 Compact IC Pro - Anion, Switzerland). H_2SO_4 was added to adjust the pH of HA,
111 HAS, and AA1 solutions, which were 4.0, 4.6, and 4.6, respectively. The pH of 4-BBA and AA2

112 solutions were 4.4 and 6.2, respectively, without adding H₂SO₄. Due to the high pH of AA2
113 solution, SO₂ concentrations in the gas/liquid phase did not reach the equilibrium even after
114 injecting higher concentrations of SO₂ for over an hour. In addition, the 4-BBA solutions were
115 degassed by bubbling pure N₂ around 30 min at a flowrate of 25 mL min⁻¹, which was also used
116 to conduct the same experiment. Meanwhile, the incoming N₂ instead of pure air went through the
117 quartz cell continuously. In all these experiments, the solutions were irradiated 50 min, except for
118 pure water (irradiated 40 min).

119 **Aerosol flow tube experiments.** Experiments were carried out at atmospheric pressure by using
120 a horizontal jacketed aerosol flow tube (AFT, 6 cm internal diameter and 180 cm length) made of
121 Pyrex. The air flowing through the reactor was kept at constant temperature of 293±1 K by means
122 of a circulating water bath. There are 5 UV-lamps (Cleo, Philips, Netherlands) surrounding the
123 flow tube with a continuous emission spectrum over 300-420 nm and a total irradiance from 0.75
124 × 10¹⁵ to 3.77 × 10¹⁵ photon cm⁻² s⁻¹, which has been described elsewhere¹⁶. 4-BBA aerosols were
125 generated from an aqueous solution (0.15 mM) by means of a constant-output atomizer (TSI Model
126 3076). A portion of the aerosol flow (~0.33 L min⁻¹) was dried using a Silica gel diffusion dryer
127 and monodispersed particle diameters of 70 or 80 nm were selected for analysis with the
128 differential mobility analyzer (DMA, TSI model 3081, impactor size 0.0508 cm), then mixed with
129 SO₂ gas (22 mL min⁻¹, ~630 ppb after mixing) and injected into the AFT. The relative humidity
130 measured at the outlet of the AFT was in the range of 25-27%. Seed particle concentration was
131 approximately 800 particles cm⁻³ and the residence time was ~15 min. A compact time of flight
132 aerosol mass spectrometer (AMS, Aerodyne Inc.) was used to sample and analyze aerosols upon
133 exiting the AFT. The obtained mass spectra were analyzed by using the AMS analysis software
134 Squirrel version 1.60P and Pika version 1.20P. Water particles instead of 4-BBA particles were

135 used as control experiments. During the control experiments, the Silica gel diffusion dryer was
136 moved from its normal position in front of the AFT to a position downstream from the AFT and
137 in the front of the AMS to allow water particles to enter the AFT without evaporation. In addition,
138 all water particles were injected into the AFT without being size selected.

139 **Pulsed laser excitation experiments.** The transient absorption spectra of the excited
140 acetophenone, flavone, xanthone, 4-BBA and HULIS (extracted from the ambient aerosols) were
141 measured using a pump-probe system described earlier¹⁷, and the experimental setup was shown
142 in Fig. S1. The third harmonic (266 nm, pulse width ~7 ns) of a Nd:YAG laser (Surelite II 10,
143 Continuum) was used as an excitation source, operating in a single-shot mode. During these
144 experiments, the laser pulse energy was limited at 10 mJ per pulse (~6 mJ cm⁻²) in order to reduce
145 the undesirable photolysis of the photosensitizer and avoid possible interferences from products.
146 To avoid any interference or electron transfer with oxygen, the photosensitizer solutions were
147 deoxygenated by bubbling argon through them for at least 20 min. The setup and principle of the
148 pulsed laser system were described in detail in the Supporting Information.

149 For the kinetic measurements, the probe wavelengths for the transient absorption decay of the
150 acetophenone, flavone, xanthone, and 4-BBA triplet state were 360, 350, 590, and 560 nm,
151 respectively, which were around the corresponding maxima in the transient absorption spectra. T*
152 extracted from the ambient aerosols had strong absorption in the wavelengths of 460, 480, and 500
153 nm, which were employed and averaged for kinetic measurements. Typically, signals from 30
154 repeated pulses were averaged for each observation wavelength.

155 All experiments were conducted under pseudo first order conditions due to a large excess of the
156 quencher (i.e., S(IV)) compared to the initial photosensitizer concentrations. The absorption decay
157 traces of the photosensitizer triplet state were fitted well with a single exponential process:

158
$$y = a + be^{-k_1 t} \quad (\text{Eq. 4})$$

159 where k_1 (s^{-1}) is the pseudo first order rate constant obtained from the slope of a logarithmic plot
160 of the transient signals, and “a” reflects potential deviation of the base line after excitation (i.e.,
161 when the absorption does not return to zero when absorbing products are produced). The lifetime
162 of T^* was defined as:

163
$$\tau = \frac{1}{k_1} \quad (\text{Eq. 5})$$

164 In the bulk aqueous experiments in this study, in order to investigate the reactivity of hydrated SO_2
165 and HSO_3^- with T^* , sodium sulfite was added into the photosensitizer solutions, then pH of the
166 solutions was decreased to 1.8 or 2.6 by adding a H_2SO_4 solution. Under these conditions, S(IV)
167 existed mainly as hydrated SO_2 and HSO_3^- . The quenching rate coefficients for T^* in the presence
168 of S(IV) were determined by the Stern-Volmer equation (Eq. 6):

169
$$-\frac{d[T^*]}{dt} = (k_0 + k_{q(\text{SO}_2 \cdot \text{H}_2\text{O})}[\text{SO}_2 \cdot \text{H}_2\text{O}] + k_{q(\text{HSO}_3^-)}[\text{HSO}_3^-])[T^*]$$

170
$$= k_{obs}[T^*] \quad (\text{Eq. 6})$$

171 where k_0 corresponds to the rate coefficient of T^* decay in the absence of oxygen or other
172 quenchers, and $k_{q(\text{SO}_2 \cdot \text{H}_2\text{O})}$ and $k_{q(\text{HSO}_3^-)}$ are the rate coefficients for the quenching by hydrated
173 SO_2 and HSO_3^- , respectively. It is important to underline that these rate constants are dependent
174 on temperature but also pH.

175

176 **Results**

177 Figure 1A shows the effect of such chemistry at 295-300 K, the diluted SO_2 gas flowing through
178 a 14 mL reactor filled halfway with aqueous solutions containing different photosensitizers, and
179 illuminated with light simulating actinic irradiation ($\lambda > 290$ nm). Various types of atmospherically
180 relevant photosensitizing chemicals were used, namely 4- (benzoyl)benzoic acid (4-BBA), humic

181 acids and their salts (HA and HAS), and finally extracts from filter samples collected in a rural
182 area (38°42' N, 115°08' E) close to Beijing during haze events in winter 2018 (AA1 and AA2,
183 which differ by their pH; pH=4.6, acidified with H₂SO₄, and 6.2, respectively). These filters were
184 shown, by UPLC/DAD/(+/-)HESI-HRMS, to be chemically complex, with more than seventy
185 carbonyl-containing compounds and a large amount of light-absorbing chromophoric compounds
186 (Fig. S2 and Database S1).

187 These solutions were initially exposed to a gaseous flow of SO₂ until steady SO₂ concentrations
188 were reached at the outlet of the reactor, with gas phase concentrations in the range from 40-100
189 ppbv. During these conditioning periods, Henry's law equilibrium and acid-base dissociation were
190 taking place, leading to the production of hydrated SO₂, HSO₃⁻ and eventually SO₃²⁻. The product
191 distribution is highly pH dependent, with SO₂ being prevalent at pH < 2, HSO₃⁻ between 3 and 6,
192 and finally SO₃²⁻ above pH=7¹⁸ (see pKa values in Eqs. 2-3).

193 Once the outlet gaseous SO₂ concentration was stabilized (with the exception of AA2 due to its
194 higher pH), the light was switched on, and for all samples, we observed a sudden loss of gas phase
195 SO₂ associated with synchronous sulfate production in the liquid phase (see Fig. 1B). Such a loss
196 is a clear indication that light initiated the conversion of hydrated SO₂ or HSO₃⁻ to SO₄²⁻, and hence
197 the oxidation proceeds from S(IV) to S(VI).

198 SO₂ consumption was not observed in the absence of the photosensitizing compounds i.e., no
199 loss on irradiated pure water. This result, combined with the poor light absorption of SO₂ in the
200 wavelength region ($\lambda > 295$ nm) considered here, shows that in this case the triplet state reaction
201 of SO₂ with water plays a minor role. We attributed the loss of gaseous SO₂ to a chemical reaction
202 between dissolved S(IV) and the photosensitizer triplet state or oxidants produced from the excited
203 state and oxygen. In fact, it has been shown that both humic acids, and 4-BBA are sources of HO₂

204 (and hence OH) radicals when exposed to light^{13, 19}. The formation of such radicals could then
205 readily react with dissolved S(IV) and lead to the observations depicted in Fig. 1. Interestingly,
206 similar trends were observed when the carrier gas was changed to pure nitrogen and all solutions
207 deoxygenated. This clearly rules out the influence of secondary oxidants, produced in the solution,
208 but point towards a direct reaction of S(IV) and the excited state of the photosensitizer.

209 To test whether such a sulfate production could also be observed under different conditions, we
210 performed aerosol flow tube experiments. Here, a bulk solution containing 4-BBA was nebulized
211 producing aerosols, then aerosols were dried, size selected (70 or 80 nm), and injected into the
212 flow tube with a residence time of ca. 15 min. SO₂ was injected at around 630 ppb in pure air
213 acting as carrier gas. At the reactor outlet, particles were chemically characterized by means of an
214 Aerosol Mass Spectrometer (AMS, Aerodyne), which is highly sensitive to sulfate. This is a
215 similar approach to the one previously used for investigating photosensitized organic aerosol
216 growth²⁰. As shown by Fig. 1C, once the lights were switched on, we observed a clear production
217 of sulfate in the particle phase, similarly to the bulk experiments above (note that due to the low
218 surface-to-volume ratio, the loss of gaseous SO₂ could not be monitored in these experiments). In
219 other words, we observed a photosensitized sulfate production, which took place within the
220 condensed phase.

221 Triplet excited states are often considered as more significant excited states in photochemistry
222 comparing to the singlet excited states, due to their longer lifetimes. Laser-flash illumination of
223 some selected photosensitizers, which are simultaneously representative of those found in
224 dissolved organic matter and biomass burning plumes (including fires for residential heating)¹³, in
225 deoxygenated aqueous solutions led to the production of the corresponding triplet state, whose
226 decay was monitored as a function of time²¹ to derive the corresponding rate constant as a function

227 of reactant concentration, pH, etc. (as detailed below). Firstly, the quenching rates of these triplet
228 states were observed to be highly pH dependent in absence of added S(IV), with acetophenone and
229 4-BBA being quenched faster under more acidic conditions, but with no obvious influences on
230 flavone and xanthone in this pH range (Fig. 2A and Fig. S3). In addition to highlighting their pH
231 dependence, those trends are useful to discriminate which S(IV) species is reactive with a given
232 T*.

233 Figure S4 shows experiments being performed by adding sodium sulfite (Na_2SO_3) into the
234 deoxygenated aqueous solutions, which redistributed into the other S(IV) compounds depending
235 on pH (their distribution in solution can be calculated based on the equilibrium Eqs. 1-3). It
236 appeared that all investigated triplet states were efficiently quenched by the presence of aqueous
237 S(IV) species but exhibited different quenching rates (see Fig. 2B and Fig. 3). Fig. 2B shows the
238 quenching rates of the triplet states in the presence of the same concentration of S(IV) but at
239 different pH i.e., with a different speciation between hydrated SO_2 and HSO_3^- . Taking into account
240 the trends shown in Fig 2A, these results indicate that the triplet state of flavone is more reactive
241 toward hydrated SO_2 , while xanthone is more reactive toward HSO_3^- (see Table S1). However, the
242 triplet states of acetophenone and 4-BBA were quenched faster under more acidic solutions, as
243 they are more reactive under acidic conditions (see Fig. 2A) and also probably more reactive
244 toward hydrated SO_2 .

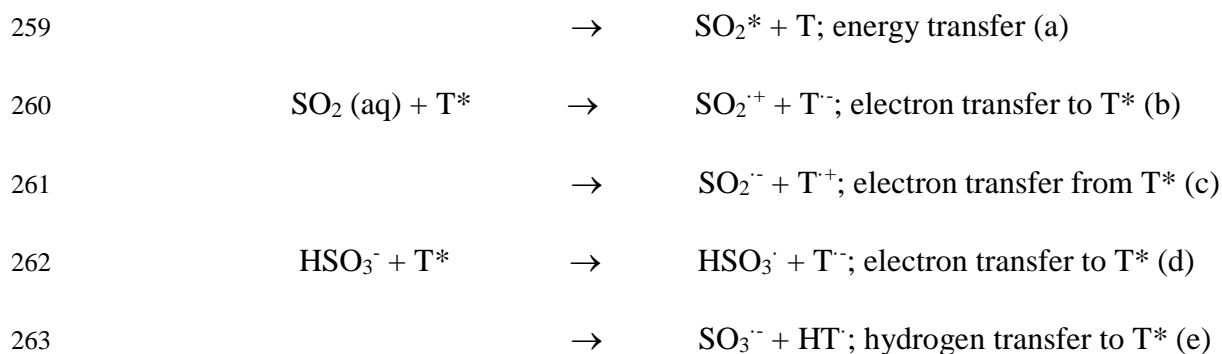
245 In the investigated pH range, both hydrated SO_2 and HSO_3^- were quenching or reacting with T*.
246 Figure 3 shows a Stern-Volmer plot of the measured quenching rates under acidic conditions where
247 hydrated SO_2 and HSO_3^- are in the dominant. In order to simplify the kinetics treatment, we
248 assumed that both S(IV) species are reacting at the same rate with the triplet state. In such a
249 simplified system, the observed quenching rate should depend linearly with the total aqueous S(IV)

250 concentration (see Fig. 3). The measured second order rate constants were all in excess of 6×10^7
251 $\text{M}^{-1}\text{s}^{-1}$, with 4-BBA being the slowest ($6.9 \times 10^7 \text{ M}^{-1}\text{s}^{-1}$) and xanthone the fastest ($1.0 \times 10^9 \text{ M}^{-1}\text{s}^{-1}$).
252 The extracts of the ambient filters from an authentic Chinese haze event also showed a reactive
253 triplet state, and quenched by S(IV) with a rate constant of $1.3 \times 10^8 \text{ M}^{-1} \text{ s}^{-1}$ (see Fig. 3).

254

255 Discussion

256 These observations can only be explained by a direct reaction between S(IV) species and the
257 studied triplet states (T^*), as the organic photodissociation is not occurring under our experimental
258 conditions with well defined photosensitizers. The possible reaction pathways are listed below:



264 All these initiation reactions are producing a sulfur containing transient compounds that will
265 start chain reactions and decay to sulfate. While we cannot, from our observations, be fully
266 conclusive on the exact reaction mechanism, one could still discuss the plausibility of each
267 pathway. Let us consider, 4-BBA as a model photosensitizer for which some information is known
268 (in contrast for instance to the authentic aerosol samples). The energy of the triplet of 4-BBA (~ 290
269 kJ mol^{-1})¹³ is slightly lower than the triplet energy of SO_2 ($\sim 300 \text{ kJ mol}^{-1}$)⁷, which cannot lead to
270 an efficient (if any) energy transfer in this case. However, one cannot rule out that for higher triplet
271 states, energy transfer could lead to a significant yield of excited state SO_2 (pathway (a)) that would
272 then react more efficiently with water, producing OH radicals and therefore led to the observed

273 oxidation process⁹. An electron transfer, either way, would therefore be the prominent pathway.
274 SO₂ has a zwitterion structure, where the sulfur is positively charged, which would prevent any
275 significant electron transfer from its electron lone-pairs. However, if produced through pathway
276 (b), SO₂⁺ might react directly with water and initiate some further radical and oxidative
277 chemistry²². Another possibility is an electron transfer to SO₂ producing SO₂⁻. It was however not
278 possible to observe the transient spectra of SO₂⁻, nor of the associated ketyl radical produced in
279 pathway (c), as the absorption of the radical anion was underlying the one of the organic
280 photosensitizer. SO₂⁻ has been previously reported to be highly reactive in aqueous solutions,
281 undergoing several reaction pathways including reactions with oxygen and typical S(IV) species,
282 ending in the production of sulfate²³⁻²⁵. In addition, HSO₃⁻ could also either transfer the electron
283 to T* producing HSO₃[·] (d) or a H-atom producing SO₃^{·-} (e), which could also continue to react
284 with oxygen and other S(IV) species to produce sulfate²³. This reaction scheme would probably
285 explain the measured quenching rates.

286 While the exact pathway is uncertain, the reaction rates are however established via the kinetics
287 observations discussed above. If we assume, that the reaction between S(IV) and T* is the rate
288 limiting step and rate coefficient is pH independent, then one can derive the associated sulfate
289 formation rates. The pH independence is arising from the assumption made that both hydrated SO₂
290 and HSO₃⁻ have similar reactivities and that the total aqueous S(IV) concentration can be used as
291 a reasonable proxy, leading to the linearity shown in Fig. 3. Details about these calculations are
292 given in the Supporting Information. It also should be noted that here particles were assumed to
293 be homogeneously mixed and in a liquid state. This chemistry (Reactions (a-e)) may then induce a
294 significant S(IV) oxidation in wet aerosols, when both SO₂ and particle phase photosensitizers,
295 such as HULIS¹⁴, levels are high. Such conditions are typically observed during Asian haze events,

296 which combine high humidity and significant anthropogenic emissions from residential burning,
297 with a contribution of up to 20 wt. % during haze events. By updating the scenario of Cheng et
298 al.¹⁰ to take into account high H₂O₂ levels recently reported²⁶, we estimated the sulfate formation
299 rate associated with SO₂ reacting with O₃, H₂O₂, TMIs, NO₂ and T* (using $1.3 \times 10^8 \text{ M}^{-1}\text{s}^{-1}$ as
300 obtained from the authentic samples) (Fig. 3). It should be noted again that we assumed that the
301 triplet states are reactive toward all S(IV) species (hydrated SO₂ and HSO₃⁻) and independent of
302 their actual pH speciation (Eqs. 1-3). To estimate the sulfate formation rate under the scenario set
303 by Cheng et al.¹⁰, we do need to estimate the particle phase concentration of triplet states under
304 steady-state haze daylight conditions. Clearly, the data related to this quantity are very limited. For
305 instance, Kaur et al.²⁷ reported very recently on such concentrations for some cleaner conditions
306 encountered in California, but with large uncertainty. While, several studies investigated the
307 amount of singlet oxygen and its ratio to coexisting triplet states in the range approximately 1¹⁰,
308 3²⁸, and 10 -100²⁷, respectively. Altogether, this leads to estimated concentrations in the range
309 from 2.3×10^{-13} to $1.6 \times 10^{-10} \text{ M}$ ²⁷. Using this range of concentrations, leads to the estimated sulfate
310 production rates shown in Fig. 4. Overall, these results show that the photosensitizing pathway
311 could make a significant contribution to the sulfate formation (Fig. 4). In the pH range from 4 to
312 6, which exactly under the conditions of Chinese haze^{29, 30}, the sulfate production rates are in the
313 range of 1.1×10^{-4} - $7.9 \mu\text{g m}^{-3} \text{ h}^{-1}$. This is a new finding that not only will help close gaps between
314 field observations and numerical models, but also may help in defining new regulations to reduce
315 sulfate formation, and hence the harmful effects of these haze events. Overall, this study also
316 stresses the knowledge gap around particle phase concentration of photosensitizing compounds
317 and the associated quantum yield for triplet state formation.

318

319 **Acknowledgments**

320 **Funding:** This project was supported by the ANR-RGC programme (project ANR-16-CE01-0013,
321 A-PolyU502/16), the European Union's Horizon 2020 research and innovation program under
322 grant agreement No. 690958 (MARSU), the Ministry of Science and Technology of China
323 (2016YFC0202700), the National Natural Science Foundation of China (91843301, 91743202),
324 and the National research program for key issues in air pollution control (DQGG0103,
325 DQGG0102). SN thanks the Université Claude Bernard Lyon 1 for providing him with a visiting
326 professorship at in the summer of 2018. CG thanks Kristopher McNeil for very helpful discussions
327 and comments on the reaction mechanism. **Competing interests:** The authors declare no
328 competing interests. **Data and materials availability:** All data to support the conclusions of this
329 manuscript are included in the main text and Supporting Information. **Supporting Information:**
330 Additional experimental details, 4 figures, 3 tables and dataset S1 were given.

331

332 **References and Notes:**

- 333 1. Albrecht, B. A., Aerosols, Cloud Microphysics, and Fractional Cloudiness. *Science* **1989**, *245*, (4923),
334 1227-1230.
- 335 2. Sedlak, D. L.; Hoigne, J., Oxidation of S(IV) in Atmospheric Water by Photooxidants and Iron in the
336 Presence of Copper. *Environmental Science & Technology* **1994**, *28*, (11), 1898-1906.
- 337 3. Warneck, P., *Chemistry of the Natural Atmosphere*. Academic Press: 2000.
- 338 4. Guo, S.; Hu, M.; Zamora, M. L.; Peng, J.; Shang, D.; Zheng, J.; Du, Z.; Wu, Z.; Shao, M.; Zeng, L.;
339 Molina, M. J.; Zhang, R., Elucidating severe urban haze formation in China. *Proc. Natl. Acad. Sci.* **2014**, *111*, (49),
340 17373-17378.
- 341 5. Wang, Y.; Zhang, Q.; Jiang, J.; Zhou, W.; Wang, B.; He, K.; Duan, F.; Zhang, Q.; Philip, S.; Xie, Y.,
342 Enhanced sulfate formation during China's severe winter haze episode in January 2013 missing from current models.
343 *J Geophys. Res. - Atm.* **2014**, *119*, (17), 10,425-10,440.
- 344 6. Hung, H.-M.; Hoffmann, M. R., Oxidation of Gas-Phase SO₂ on the Surfaces of Acidic Microdroplets:
345 Implications for Sulfate and Sulfate Radical Anion Formation in the Atmospheric Liquid Phase. *Environ. Sci. Tech.*
346 **2015**, *49*, (23), 13768-13776.
- 347 7. Donaldson, D. J.; Kroll, J. A.; Vaida, V., Gas-phase hydrolysis of triplet SO₂: A possible direct route to
348 atmospheric acid formation. *Scientific Reports* **2016**, *6*, 30000.
- 349 8. Kroll, J. A.; Frandsen, B. N.; Kjaergaard, H. G.; Vaida, V., Atmospheric Hydroxyl Radical Source:
350 Reaction of Triplet SO₂ and Water. *The Journal of Physical Chemistry A* **2018**, *122*, (18), 4465-4469.
- 351 9. Martins-Costa, M. T. C.; Anglada, J. M.; Francisco, J. S.; Ruiz-López, M. F., Photochemistry of SO₂ at the
352 Air-Water Interface: A Source of OH and HOSO Radicals. *J. Am. Chem. Soc.* **2018**, *140*, (39), 12341-12344.

- 353 10. Cheng, Y.; Zheng, G.; Wei, C.; Mu, Q.; Zheng, B.; Wang, Z.; Gao, M.; Zhang, Q.; He, K.; Carmichael, G.;
354 Pöschl, U.; Su, H., Reactive nitrogen chemistry in aerosol water as a source of sulfate during haze events in China.
355 *Science Advances* **2016**, 2, (12), e1601530.
- 356 11. Li, L.; Hoffmann, M. R.; Colussi, A. J., Role of Nitrogen Dioxide in the Production of Sulfate during
357 Chinese Haze-Aerosol Episodes. *Environ. Sci. Tech.* **2018**, 52, (5), 2686-2693.
- 358 12. George, C.; Ammann, M.; D'Anna, B.; Donaldson, D. J.; Nizkorodov, S. A., Heterogeneous
359 Photochemistry in the Atmosphere. *Chem. Rev.* **2015**, 115, (10), 4218-4258.
- 360 13. McNeill, K.; Canonica, S., Triplet state dissolved organic matter in aquatic photochemistry: reaction
361 mechanisms, substrate scope, and photophysical properties. *Environmental Science: Processes & Impacts* **2016**, 18,
362 (11), 1381-1399.
- 363 14. Baduel, C.; Monge, M. E.; Voisin, D.; Jaffrezo, J. L.; George, C.; El Haddad, I.; Marchand, N.; D'Anna,
364 B., *Environ. Sci. Technol.* **2011**, 45, 5238.
- 365 15. Ciuraru, R.; Fine, L.; van Pinxteren, M.; D'Anna, B.; Herrmann, H.; George, C., Photosensitized
366 production of functionalized and unsaturated organic compounds at the air-sea interface. *Scientific Reports* **2015**, 5,
367 12741.
- 368 16. Dupart, Y.; King, S. M.; Nekat, B.; Nowak, A.; Wiedensohler, A.; Herrmann, H.; David, G.; Thomas, B.;
369 Miffre, A.; Rairoux, P.; D'Anna, B.; George, C., Mineral dust photochemistry induces nucleation events in the
370 presence of SO₂. *Proc. Natl. Acad. Sci.* **2012**, 109, (51), 20842-20847.
- 371 17. Jammoul, A.; Dumas, S.; D'Anna, B.; George, C., Photoinduced oxidation of sea salt halides by aromatic
372 ketones: a source of halogenated radicals. *Atmos. Chem. Phys.* **2009**, 9, (13), 4229-4237.
- 373 18. Seinfeld, J. H.; Pandis, S. N., *Atmospheric Chemistry and Physics: From Air Pollution to Climate Change*.
374 Wiley: 2006.
- 375 19. Canonica, S.; Jans, U.; Stemmler, K.; Hoigne, J., *Environ. Sci. Technol.* **1995**, 29, 1822.
- 376 20. Monge, M. E.; Rosenørn, T.; Favez, O.; Müller, M.; Adler, G.; Abo Riziq, A.; Rudich, Y.; Herrmann, H.;
377 George, C.; D'Anna, B., Alternative pathway for atmospheric particles growth. *Proc. Natl. Acad. Sci.* **2012**, 109, (18),
378 6840-6844.
- 379 21. Tinel, L.; Rossignol, S.; Ciuraru, R.; Dumas, S.; George, C., Photosensitized reactions initiated by 6-
380 carboxypterin: singlet and triplet reactivity. *Physical Chemistry Chemical Physics* **2016**, 18, (25), 17105-17115.
- 381 22. Cartoni, A.; Catone, D.; Bolognesi, P.; Satta, M.; Markus, P.; Avaldi, L., HSO₂⁺ Formation from Ion-
382 Molecule Reactions of SO₂⁺ with Water and Methane: Two Fast Reactions with Reverse Temperature-Dependent
383 Kinetic Trend. *Chemistry – A European Journal* **2017**, 23, (28), 6772-6780.
- 384 23. Neta, P.; Huie, R. E.; Harriman, A., One-electron-transfer reactions of the couple SO₂/SO₂⁻ in aqueous-
385 solutions - pulse radiolytic and cyclic voltammetric studies. *J. Phys. Chem.* **1987**, 91, (6), 1606-1611.
- 386 24. Burlamacchi, L.; Guarini, G.; Tiezzi, E., Mechanism of decomposition of sodium dithionite in aqueous
387 solution. *Trans. Faraday Soc.* **1969**, 65, (554P), 496-502.
- 388 25. Rinker, R. G.; Gordon, T. P.; Mason, D. M.; Sakaida, R. R.; Corcoran, W. H., Kinetics and mechanism of
389 the air oxidation of the dithionite ion (S₂O₄²⁻) in aqueous solution. *J. Phys. Chem.* **1960**, 64, (5), 573-581.
- 390 26. Ye, C.; Liu, P.; Ma, Z.; Xue, C.; Zhang, C.; Zhang, Y.; Liu, J.; Liu, C.; Sun, X.; Mu, Y., High H₂O₂
391 Concentrations Observed during Haze Periods during the Winter in Beijing: Importance of H₂O₂ Oxidation in
392 Sulfate Formation. *Environ. Sci. Technol.* **2018**, 5, (12), 757-763.
- 393 27. Kaur, R.; Labins, J. R.; Helbock, S. S.; Jiang, W.; Bein, K. J.; Zhang, Q.; Anastasio, C. Photooxidants from
394 Brown Carbon and Other Chromophores in Illuminated Particle Extracts. *Atmos. Chem. Phys.* **2019**, 19 (9), 6579–
395 6594.
- 396 28. Kaur, R.; Anastasio, C., First Measurements of Organic Triplet Excited States in Atmospheric Waters.
397 *Environ. Sci. Tech.* **2018**, 52, (9), 5218-5226.
- 398 29. Song, S.; Gao, M.; Xu, W.; Shao, J.; Shi, G.; Wang, S.; Wang, Y.; Sun, Y.; McElroy, M. B., Fine-particle
399 pH for Beijing winter haze as inferred from different thermodynamic equilibrium models. *Atmos. Chem. Phys.* **2018**,
400 18, (10), 7423-7438.
- 401 30. Ding, J.; Zhao, P.; Su, J.; Dong, Q.; Du, X., Aerosol pH and its influencing factors in Beijing. *Atmos.*
402 *Chem. Phys. Discuss.* **2018**, 2018, 1-34.

403

404

405

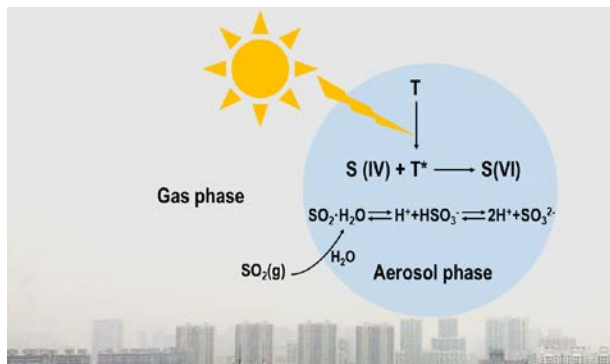
406

Figures

407

Abstract Art

408

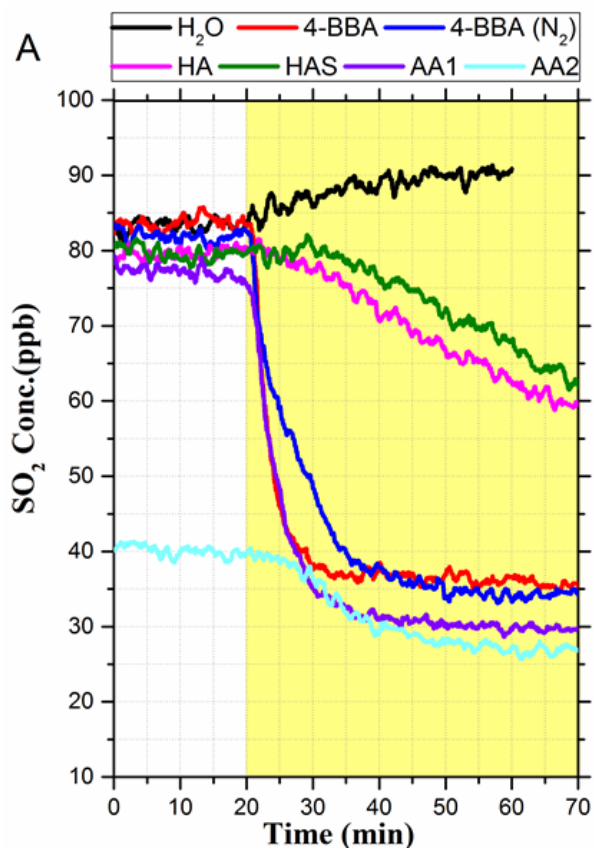


409

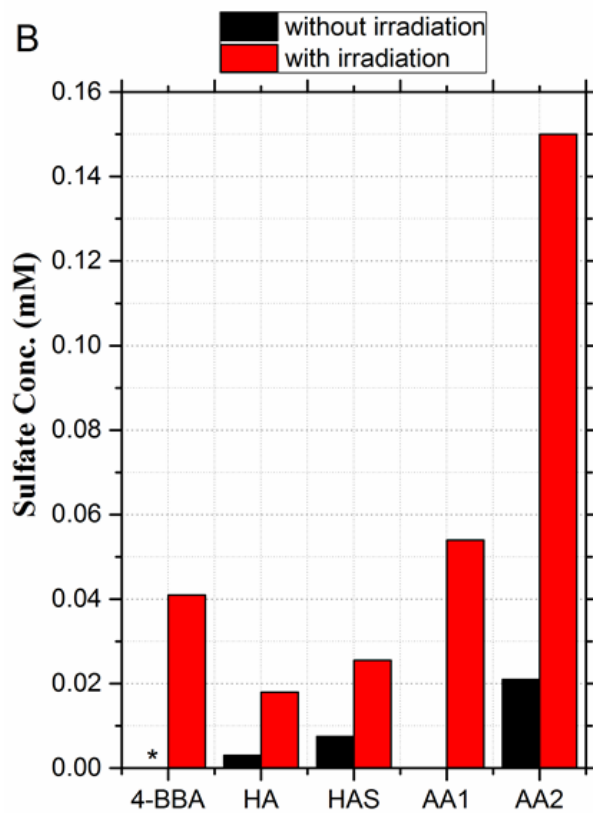
410

411

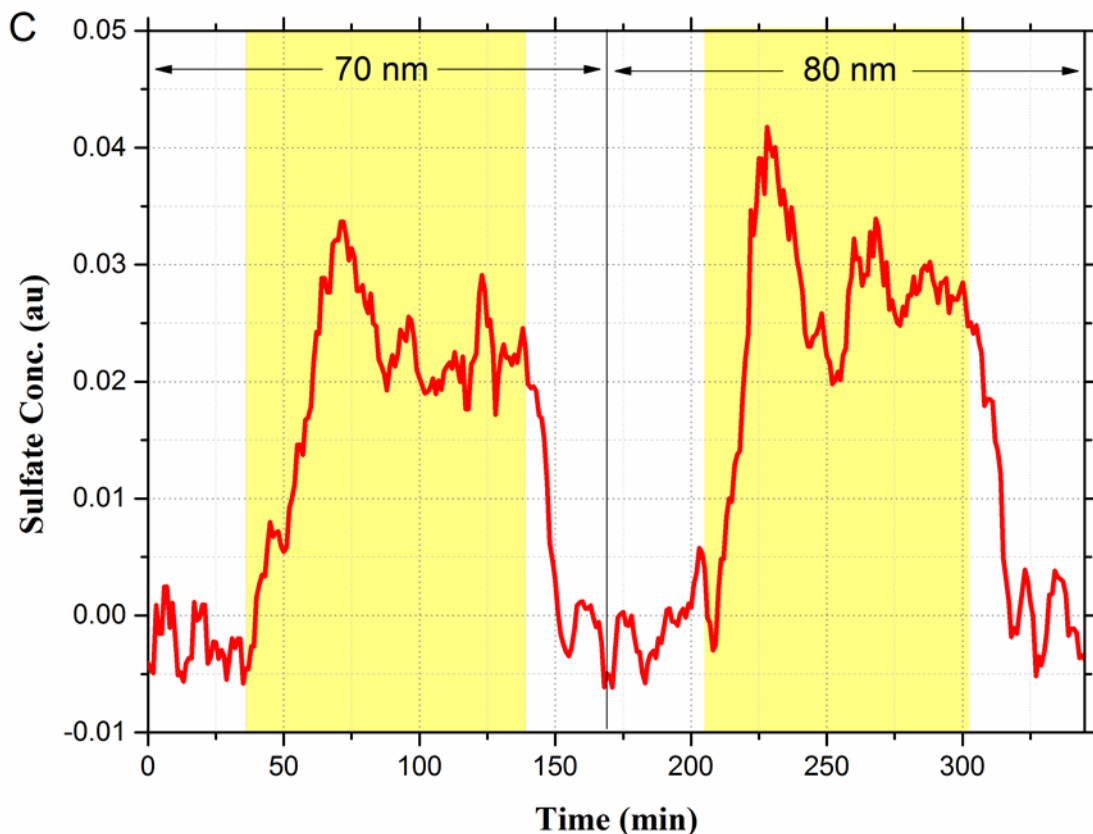
412



413

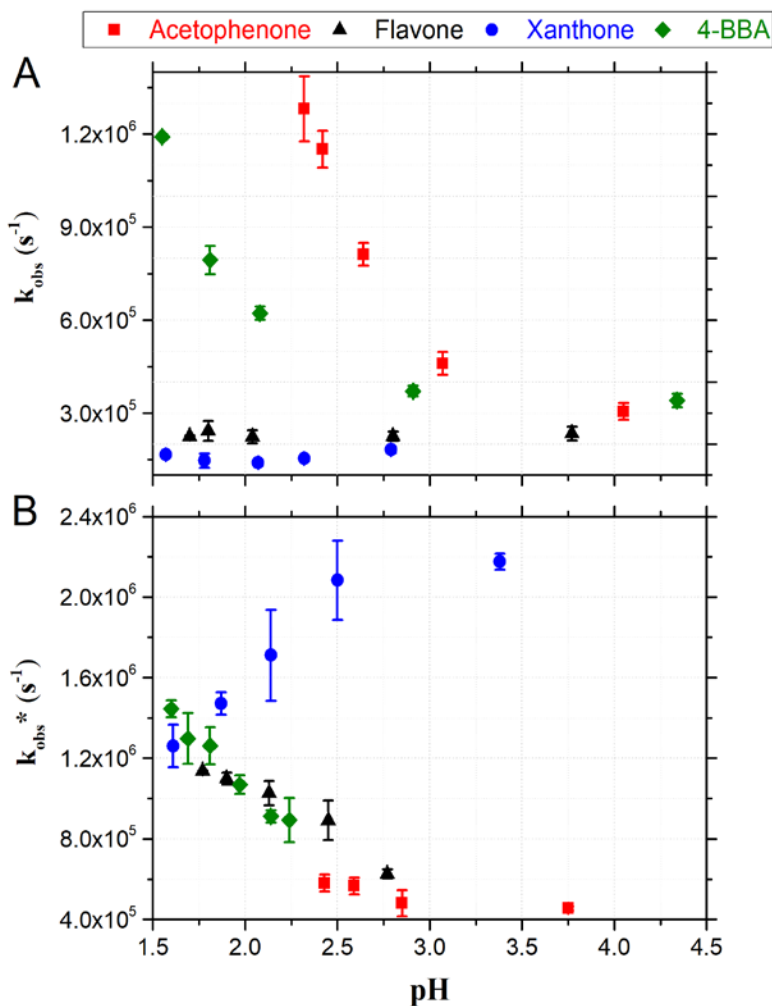


414
415
416



417
418
419
420
421
422
423

Fig. 1. SO₂ loss and sulfate formation. (A) Time traces of gaseous SO₂ loss above aqueous solutions of 4-BBA, HA, HAS AA1, and AA2. (B) Corresponding sulfate production. AA1 and AA2 differ by their pH and hence their capacity to store S(IV). Sulfate concentrations were blank-corrected for the HA, HAS, AA1 and AA2 experiments. * The concentration was below detection limit. (C) Sulfate production measured by an aerosol mass spectrometer in 4-BBA particles with diameters of 70 and 80 nm in the aerosol flow tube. Residence time is 15 min.



425

426 **Fig. 2. The pH influence on the quenching rates of the triplet states in the absence (A) and**
 427 **presence (B) of S(IV).** Red squares, acetophenone, 0.25 mM sodium sulfite; black triangles,
 428 flavone, 0.1 mM sodium sulfite; blue circles, xanthone, 1 mM sodium sulfite; green diamonds, 4-
 429 BBA, 20 mM sodium sulfite. k_{obs}^* is the blank-corrected quenching rates, which means here these
 430 values obtained from the triplet states being quenched only by S(IV). It should be noted that here
 431 xanthone concentrations were different from other xanthone experiments in this study.

432

433

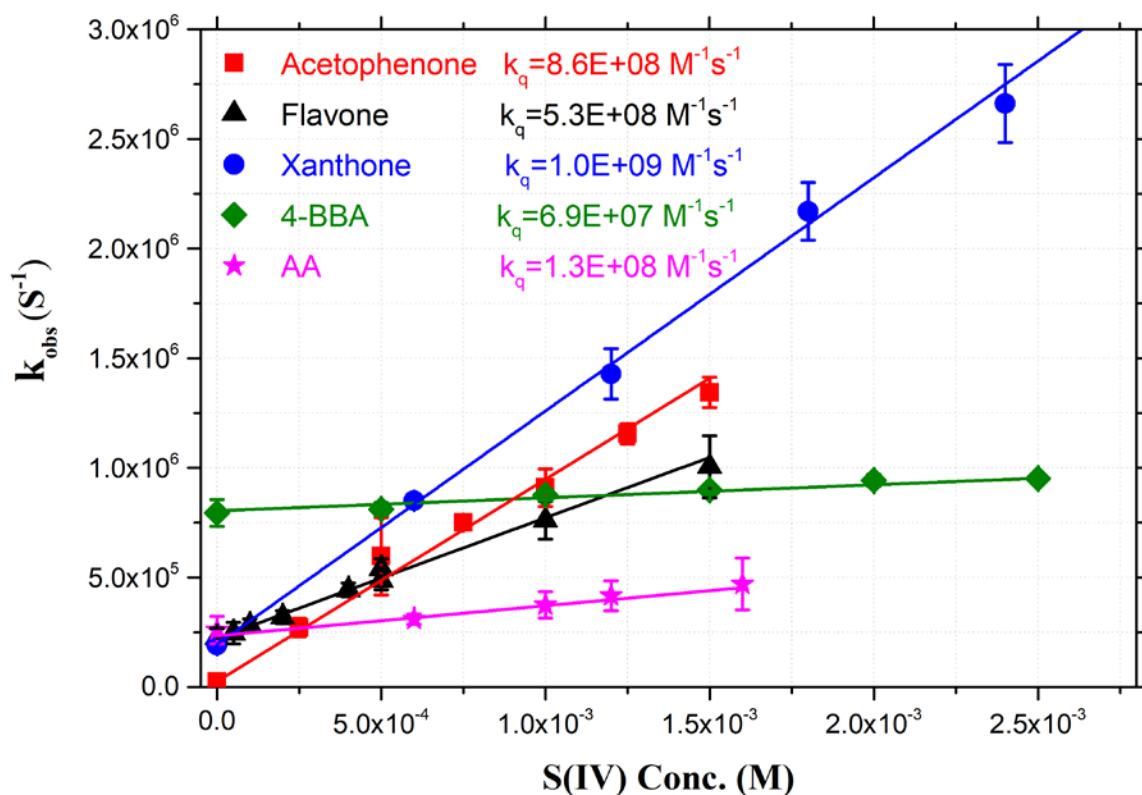
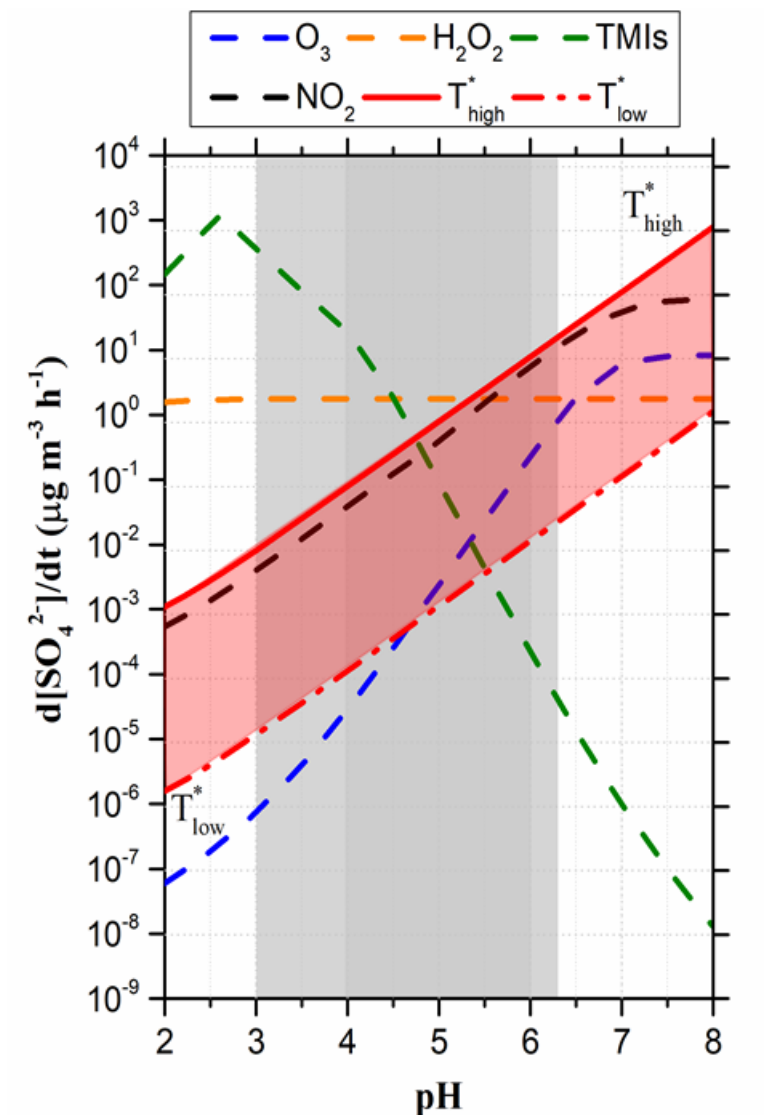


Fig. 3. Stern–Volmer plots of the observed quenching first-order rate coefficients k_{obs} as a function of aqueous S(IV) concentration. Red squares, acetophenone; black triangles, flavone; blue circles, xanthone; green diamonds, 4-BBA; pink stars, HULIS-AA. The pH of all acetophenone solutions is 2.6 and the pH of all flavone, xanthone, 4-BBA, and HULIS-AA solutions is 1.8.

434
435
436
437
438
439
440
441



442
 443
 444
 445
 446
 447
 448

Fig. 4. Sulfate production rates for Beijing winter haze calculated for main aqueous-phase reaction pathways versus pH. The blue, orange, green, and black lines represent O_3 , H_2O_2 , TMI, and nitrogen dioxide (NO_2) pathways, respectively, from Cheng et al.¹⁰. The red region represents the photosensitized oxidation. Gray-shaded areas indicate characteristic pH ranges during haze episodes in China, with the darker ones being more common^{29, 30}.